Proceedings of the 5th Joint ASME/JSME Fluids Engineering Conference
July 30-August 2, 2007, San Diego, CA, USA

FEDSM2007-37298

ASSESSMENT OF DES MODELS FOR SEPARATED FLOW FROM A HUMP IN A TURBULENT BOUNDARY LAYER

Daniel C. Lyons
Applied Research Laboratory
Dept. of Mechanical and Nuclear Engineering
Penn State University, State College, Pa
dcl155@psu.edu

Leonard J. Peltier
Applied Research Laboratory
Dept. of Mechanical and Nuclear Engineering
Penn State University, State College, Pa
peltierlj@psu.edu

Frank J. Zajaczkowski
Applied Research Laboratory
Penn State University, State College, Pa
fxz101@ psu.edu

Eric G. Paterson
Applied Research Laboratory
Dept. of Mechanical and Nuclear Engineering
Penn State University, State College, Pa
egp11@ psu.edu

ABSTRACT

Turbulent flow past the Glauert-Goldschmied body, a flow-control hump in a turbulent boundary layer, is studied numerically using detached-eddy simulation (DES), zonal detached-eddy simulation (ZDES), delayed detached-eddy simulation (DDES), and Reynolds-Averaged Navier-Stokes (RANS) modeling. The geometry is smooth so the downstream separation point is not set by facets of the geometry but is a function of the pressure gradient, a challenging condition for turbulence models. Comparisons to experimental data show that RANS with the Spalart-Allmaras turbulence model predicts the mean-field statistics well. The ZDES and DDES methods perform better than the DES formulation and are comparable to RANS in most statistics. An analysis of model behavior indicates that modeled stress depletion in the detached shear layer shortly after separation leads to loss of accuracy in the DES variants.

INTRODUCTION

Computational fluid dynamics (CFD) is today a primary analysis and design tool in engineering. The success of CFD is due not only to rapidly expanding computational resources but also to increased fidelity of modern numerical models such as DES. Recent advances in modeling turbulent flows have involved classes of eddy-resolving techniques that blend statistical RANS modeling near walls with Large-Eddy Simulation (LES) in outer regions of interest. Detached-Eddy Simulation (Spalart et al., 1997) and its variants are perhaps the most common examples. DES of massively separated flows (Strelets, 2001) has been successful in yielding improved flow statistics. The level of success of DES approaches for non-massively separated flows, however, is not clear.

This work is motivated by the earlier study of Paterson and Peltier (2005) who document deficiencies of DES in modeling trailing-edge flows for airfoils where the separation point is not imposed by the geometry. They found that when the transition from RANS to DES occurs upstream of the separation point, resolved turbulence scales do not evolve quickly enough to compensate for the loss of statistical turbulence leading to a region of depleted turbulence stresses and unphysical flow that influences the flow downstream. Spalart et al. (2006) have used the term “modeled-stress depletion” to identify this difficulty and Menter, Kuntz, and Bender (2003) discuss the resulting effect of “grid-induced separation.” Variants of DES have been developed that provide boundary-layer shielding automatically. DDES (Spalart, et al., 2006) and ZDES (Slimon, 2003) are examples.

The purpose of this work is to evaluate RANS, DES, ZDES and DDES for simulation of a separated flow where the separation point is not prescribed by sharp edges in the geometry. The Glauert-Goldschmied body embedded in a turbulent boundary layer is our test case. The geometry comprises a nominally 2D hump in a channel with a smooth curved surface on the leeward side where separation occurs. A detailed experimental database is available from NASA (http://cfdval2004.larc.nasa.gov/case3.html) for code validation purposes. These data and corresponding computational studies have been extensively documented in literature already, see Seifert and Pack (2002), Rumsey, Gatski, Sellers, Vatsa, and Viken (2004), Krishnan, Squires, and Forsythe (2004), and Biswas (2006), among others.

This manuscript presents details of the Glauert-Goldschmied body. The governing equations and descriptions of the turbulence closures are then presented, followed by the flow solver and computational grid. Comparisons to experimental data and differences between the DES and RANS models are discussed and the paper concludes with a summary of results.

THE GLAUERT-GOLDSCHMIED BODY AND TEST CONDITIONS

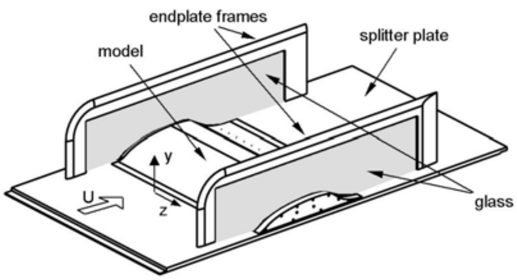

Figure 1 Schematic of hump model used for CFD (download from http://cfdval2004.larc.nasa.gov/case3.html).

The Glauert-Goldschmied Body is a 2-D hump mounted in a parallel channel (see schematic in Fig. 1). End plates are used in the test section to remove the channel's side-wall boundary layers, and a splitter plate is used to place the configuration above the boundary layer at the floor of the channel and to provide a nearly constant inflow velocity to the test section. The hump chord length is c=16.536 inches (0.42 m), and the hump height is 2.116 inches (0.0537 m). The distance from the splitter plate to the top wall of the channel is 15.032 inches (0.382 m).

A rich experimental data base is available for this configuration (http://cfdval2004.larc.nasa.gov/case3.html). The experimental measurements consist of x and y velocities in the recirculation region (Greenblatt, Paschal, Yao, Harris, Schaeffler, and Washburn, 2004) and pressure and shear stress measurements (Naughton, Viken, and Greenblatt, 2004) along the bottom surface of the hump. The results have been used for CFD validation during CFDVAL 2004. RANS, DES, LES, and DNS models were applied. The documentation of the validation exercises is available in the literature.

We consider the baseline case from the NASA test. The freestream velocity is U=34.6 m/s. The reported dynamic viscosity and density are μ=18.4x10^{-6} kg/ms and ρ=1.184 kg/m^3, yielding a chord Reynolds number of Re=936,000. Experimental data show that the flow statistics are nominally 2D and that separation occurs on the leeward side of the hump at x/c=0.665, measured from the upstream edge of the hump geometry, creating a detached shear layer followed by reattachment downstream of the separation point at x/c=1.11.

The primary goals of this work are to provide documentation of the performance of ZDES and DDES relative to RANS and DES and to explain model deficiencies.

GOVERNING EQUATIONS

Navier-Stokes Equations

The equations governing fluid flow are the Navier-Stokes momentum conservation equations and continuity,

$$\frac{\partial \tilde{u}_i}{\partial t} + \tilde{u}_j \frac{\partial \tilde{u}_i}{\partial x_j} = -\frac{1}{\rho}\frac{\partial \tilde{p}}{\partial x_i} + \nu \frac{\partial^2 \tilde{u}_i}{\partial x_j \partial x_j} \text{ and } \frac{\partial \tilde{u}_i}{\partial x_i} = 0 \qquad (1)$$

where $\tilde{u}_i$ is the velocity field and $\tilde{p}$ is pressure. The notation follows Tennekes and Lumley (1972), where the overset tilde denotes a full variable, one that has both a statistical mean value and a fluctuating component,

$$\tilde{u}_i = U_i + u_i \text{ and } \tilde{p} = P + p\,. \qquad (2)$$

Filtered Navier-Stokes Equations

In general, CFD models do not "resolve" all turbulence motions for high Reynolds number flows in geometrically complicated environments. Instead, CFD models solve for a "filtered"/"resolved" variable ($\tilde{u}_i^r$ and $\tilde{p}^r$) modeling the effects of the "subfilter" ($\tilde{u}_i^s$ and $\tilde{p}^s$) motions. One can formally filter the Navier-Stokes momentum conservation equations and continuity to derive the governing equations solved by a CFD code:

$$\frac{\partial \tilde{u}_i^r}{\partial t} + \tilde{u}_j^r \frac{\partial \tilde{u}_i^r}{\partial x_j} = -\frac{1}{\rho}\frac{\partial \tilde{p}}{\partial x_i} + \nu \frac{\partial^2 \tilde{u}_i^r}{\partial x_j \partial x_j} - \frac{\partial \tilde{\tau}_{ij}}{\partial x_j} \text{ and } \frac{\partial \tilde{u}_i^r}{\partial x_i} = 0\,; \qquad (3)$$

where $\tau_{ij} \equiv (u_i^r u_j^s + u_i^s u_j^r + u_i^s u_j^s)^r + (u_i^r u_j^r)^r - (u_i^r u_j^r)$ is the "subfilter" stress which must be modeled.

An eddy-diffusivity model is used that relates the deviatoric "subfilter" stress, $\tilde{\tau}_{ij}^D \equiv \tilde{\tau}_{ij} - \frac{1}{3}\tilde{\tau}_{kk}\delta_{ij}$, to the resolved strain through a scalar eddy diffusivity, ν_T:

$$\tilde{\tau}_{ij}^D \equiv -2\nu_T S_{ij}^r \text{, where } \tilde{S}_{ij}^r \equiv \frac{1}{2}\left(\frac{\partial \tilde{u}_i^r}{\partial x_j} + \frac{\partial \tilde{u}_j^r}{\partial x_i}\right) \qquad (4)$$

The non-deviatoric component of the stress tensor is absorbed into a modified pressure

$$\hat{\tilde{p}} \equiv \tilde{p} + \frac{1}{3}\rho \tilde{\tau}_{kk}\,. \qquad (5)$$

yielding

$$\frac{\partial \tilde{u}_i^r}{\partial t} + \tilde{u}_j^r \frac{\partial \tilde{u}_i^r}{\partial x_j} = -\frac{1}{\rho}\frac{\partial \hat{\tilde{p}}}{\partial x_i} + 2\frac{\partial}{\partial x_j}\left[\left(\nu + \nu_T\right)\tilde{S}_{ij}^r\right], \qquad (6)$$

where ν_T must be modeled.

Modeling Strategies

RANS, DES, DDES and ZDES are evaluated. The flow solver is modified to accommodate these models solely through the eddy diffusivity closure.

Spalart-Allmaras RANS

Our RANS closure is the Spalart-Allmaras (SA), one-equation turbulence model (Spalart and Allmaras, 1992). The SA model relates the eddy diffusivity, ν_T, to a computed diffusivity, $\tilde{\nu}$, that satisfies the transport equation:

$$\frac{\partial \tilde{\nu}}{\partial t} + U_j \frac{\partial \tilde{\nu}}{\partial x_j} = c_{b1}\tilde{S}\tilde{\nu} - c_{w1} f_w \left(\frac{\tilde{\nu}}{d}\right)^2 + \frac{1}{\sigma}\frac{\partial}{\partial x_k}\left[\left(\nu + \tilde{\nu}\right)\frac{\partial \tilde{\nu}}{\partial x_k}\right] + \frac{c_{b2}}{\sigma}\frac{\partial \tilde{\nu}}{\partial x_k}\frac{\partial \tilde{\nu}}{\partial x_k}, \qquad (7a)$$

where d is the distance to the nearest no-slip surface. The model constants are

$$\begin{aligned} &c_{b1} = 0.1355 \quad c_{b2} = 0.622 \quad c_{v1} = 7.1 \quad \sigma = \frac{2}{3} \\ &c_{w1} = \frac{c_{b1}}{\kappa^2} + \frac{\left(1 + c_{b2}\right)}{\sigma} \quad c_{w2} = 0.3 \quad c_{w3} = 2 \quad \kappa = 0.41 \end{aligned}, \qquad (7b)$$

and the model functions are

$$\begin{aligned} &f_{v1} = \frac{\chi^3}{\chi^3 + c_{v1}^3} \quad f_{v2} = 1 - \frac{\chi}{1 + \chi f_{v1}} \quad f_w = g\left(\frac{1 + c_{w3}^6}{g^6 + c_{w3}^6}\right)^6 \\ &\chi = \frac{\tilde{\nu}}{\nu} \quad g = r + c_{w2}\left(r^6 - r\right) \quad r = \frac{\tilde{\nu}}{\tilde{S}\left(\kappa d\right)^2} \\ &S = \sqrt{2\Omega_{ij}\Omega_{ij}} \quad \tilde{S} = S + \frac{\tilde{\nu}}{\left(\kappa d\right)^2} f_{v2} \quad \Omega_{ij} = \frac{1}{2}\left(\frac{\partial U_i}{\partial x_j} - \frac{\partial U_j}{\partial x_i}\right) \end{aligned}. \qquad (7c)$$

The SA model diagnoses the time scale of the turbulence from the mean field vorticity and chooses the characteristic length of maximum distance to the wall. The model constants and functions are tuned to data. Experience with the SA model suggests that for many flow fields, the one equation model performs as well as contemporary two-equation models for wall-bounded flows.

Detached-Eddy Simulation (DES)

The baseline DES model is derived from the SA RANS closure by replacing the characteristic length scale d with a hybrid length scale $\tilde{d}$, where $\tilde{d}$ is defined as the minimum of d and a characteristic grid scale, $C_{DES}\Delta$:

$$\tilde{d} = \min(d, C_{DES}\Delta). \qquad (8)$$

The destruction term in (7a) is proportional to the inverse of the characteristic length scale, d ($\tilde{d}$ for DES). Therefore smaller values of $\tilde{d}$ lead to increased destruction resulting in smaller diffusivities, $\tilde{\nu}$ and ν_T. The interpretation is that if a flow is well resolved ($C_{DES}\Delta << d$) the unresolved turbulence mixing is similarly small, so the modeled turbulence mixing should be small too, i.e. small $\tilde{\nu}$. When turbulence fluctuations are unresolved, as in RANS, the unresolved mixing is all of the turbulence mixing, so the modeled mixing should be large, i.e. large $\tilde{\nu}$. In (7a), large d yields low destruction thus yielding larger values of $\tilde{\nu}$, as desired.

Zonal Detached-Eddy Simulation (ZDES)

The DES model as described in (7a) coupled with (8) discriminates RANS regions from LES ones, solely on the relative length scale ratio, $C_{DES}\Delta / d$. When $C_{DES}\Delta << d$, the DES model is allowed to transition to LES, even within boundary layers where one would like to remain RANS. Slimon's (2003) ZDES introduces a discriminator function ψ designed to identify boundary layers $\psi \le 1$ thereby allowing control of the transition from RANS to DES in these regions:

$$\psi = \min\left(\frac{1}{2} d \frac{C_\mu \Omega}{a_1 k^{1/2}}, \frac{d^2\Omega}{500\nu}\right). \qquad (9a)$$

Slimon (2003) uses the model constants

$$a_1 = 0.31 \quad C_\mu = 0.09 \qquad (9b)$$

and approximates the turbulent kinetic energy, k, as

$$k \approx \max\left(\frac{\nu_T}{a_1} S, k_0\right). \qquad (9c)$$

k_0 is a freestream value (note: (9c) corrects a typographical error in Slimon, 2003). He also reports that numerical experiments showed that best results were obtained when $f_{v1} = f_w = 1$ and $f_{v2} = 0$, values also adopted here.

Given the ability to discriminate attached boundary layers through the black/white function ψ, ZDES modifies the DES definition for the characteristic model length scale $\tilde{d}$, such that

$$\tilde{d} = \begin{cases} d & \text{for } \psi \le 1 \\ \min(d, C_{DES}\Delta) & \text{for } \psi > 1 \end{cases} \qquad (10)$$

The method is zonal in the sense that it sharply delineates RANS and DES regions, however, the governing equations are continuous across the ZDES interface ensuring a smooth solution.

Delayed-Detached-Eddy Simulation (DES)

DDES also replaces the length scale d in the SA model with a modified length scale $\tilde{d}$ and, like ZDES, uses a discriminator function, f_d, to distinguish the RANS and LES regions:

$$\tilde{d} \equiv d - f_d \max(0, d - C_{DES}\Delta) \qquad (11)$$

where

$$f_d \equiv 1 - \tanh([8r_d]^3)\,. \qquad (12)$$

The new parameter r_d replaces the parameter r in the original SA RANS formulation,

$$r_d \equiv \frac{\nu_t + \nu}{\sqrt{U_{i,j}U_{i,j}}\,\kappa^2 d^2}\,. \qquad (13)$$

Through the deformation tensor magnitude in the denominator, r_d is sensitive to both strain and rotation.

NUMERICAL METHOD AND COMPUTATIONAL GRID

Numerical Method

AcuSolve, a commercial flow solver, was used to perform the calculations in this study. AcuSolve is a finite-element flow solver that is second-order accurate in space and time. The code imports a number of grid formats. Fluent case files were the primary interchange format used between the grid generation code, GridGen, and AcuSolve during this study. The code implements a broad range of boundary conditions and is richly instrumented with data monitoring and data extraction tools. Experience at ARL with the code confirms that it is robust and accurate for the single phase, incompressible, RANS and DES cases investigated. The data structure is a hybrid of C routines comprising the data flow backbone of the code with Fortran77 routines to handle numerically intensive operations.

Computational Grid and Boundary Conditions

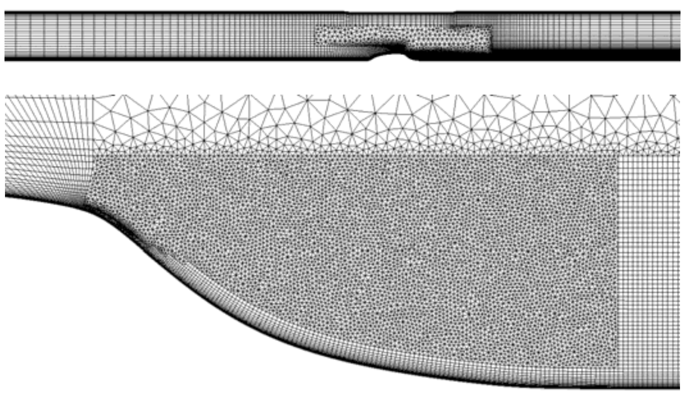

Figure 2 Full view (above) and close up (below) of the computational grid.

To guide our mesh generation, we follow the results of Krishnan et al. (2004) who report a complete mesh resolution and time-step sensitivity study defining minimum grid spacings and time-step size to resolve the physics of this flow adequately. Our mesh is an unstructured grid comprising brick and wedge elements. To construct our mesh, we first build a 2D mesh of triangles and quadrangles that resolve the relevant details of the flow and flow geometry (see Fig. 2). High grid resolution is placed in the recirculation region on the lee side of the hump where turbulence is to be resolved (Fig. 2, lower). To capture the separation point, grid density is increased near *x/c*=0.65 where separation is expected. The 3D mesh is generated from the 2D mesh by extrusion in the spanwise direction.

The grid cells in the turbulence-resolving recirculation region are isotropic. The grid spacing is $\Delta x/c=\Delta y/c=\Delta z/c$=0.003025, similar to Krishnan et al.'s (2004) guidelines. The 3D mesh extends 40 cells in the spanwise direction yielding a mesh depth of *z/c*=0.121, which is slightly under 10% of the width of the geometry. The inlet is placed upstream of the hump at *x/c*=-6.8 where slug flow conditions are applied. This location is chosen because it yields a developing boundary layer that matches experimental data at *x/c*=-2.1, as seen in the left panel of Fig. 3. A time-step size of Δt=.0032 *c/U* is used, a value found by Krishnan et al. (2004) to resolve the low to mid frequencies of turbulence spectra. The downstream outlet is at *x/c*=6.0. The upper and lower walls are no-slip surfaces. Periodic conditions are enforced in the spanwise direction.

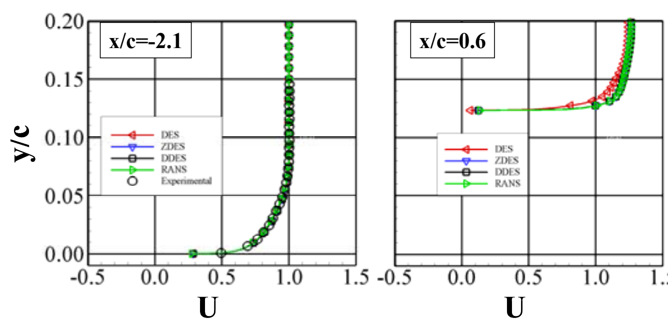

Figure 3 U velocity profiles for region near inflow (x/c=-2.14) for DES, ZDES, DDES, RANS and experiment and prior to DES separation (x/c=0.6) for DES, ZDES, DDES and RANS.

RESULTS AND DISCUSSION

In this section, we compare our CFD solutions to NASA's baseline (no flow control) configuration to assess the strengths and weaknesses of RANS and the DES variants for modeling a non-massively separated flow.

Figure 4 Isosurfaces of Q-criterion for ZDES and RANS.

Modeled-Stress Depletion

DES approaches resolve the largest scales of turbulence in their LES zone, the separated region for the Glauert-Goldschmied flow, so flow statistics must be collected. Instantaneous turbulence eddies resolved in one snapshot from the ZDES solution (Fig. 4, upper panel) are visualized using isosurfaces of Q-criterion (Lesieur, Metais, and Comte, 2005). The result is a complicated mass of interacting vortices in the separated zone and downstream into the recovery region. The statistical recirculation on the lee side of the hump is not readily discerned. The RANS solution (Fig. 4, lower panel) shows that the flow statistics are characterized by a dominant, spanwise vortical structure on the lee side of the hump representing the statistical recirculating separated zone. To compute similar flow statistics from the DES-based methods, averaging in time and space is used. In this study, the eddy-resolving flows are integrated until a statistically stationary state is reached, about 7000 time steps, then time-averaged statistics are collected over 4000 time steps, a dimensionless time of 12.8 equivalent to approximately 28 separation-bubble passage times, which are further averaged spatially across the span (a homogeneous direction).

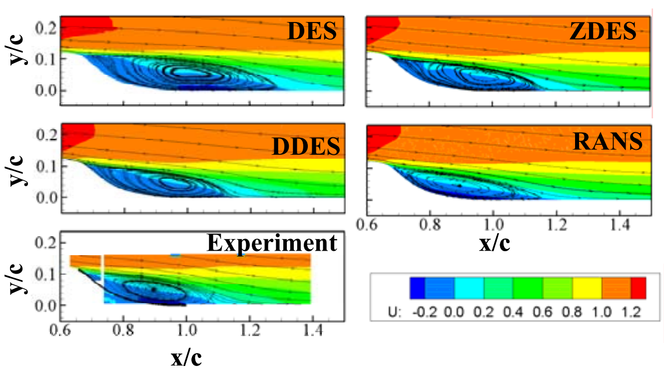

Figure 5 Streamline and x-velocity contour of DES, DDES, ZDES, RANS and experiment.

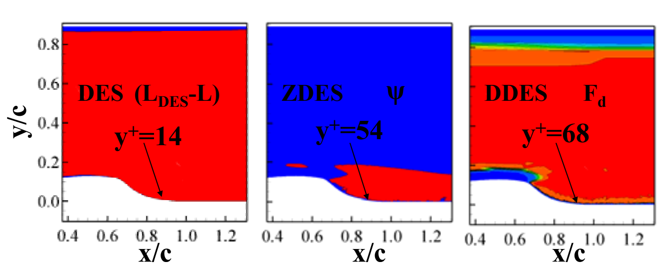

Figure 6 Full view of RANS/LES regions for DES methods with blue indicating RANS and red indicating LES. Y plus values indicate approximately where the flow transitions from RANS to LES.

Color contours of the mean longitudinal velocity, *U*, with streamlines to detail the statistical separated zone are presented in Fig. 5 for DES, ZDES, DDES, RANS and the experiment. Table 1 shows the separation and reattachment. The experimental separation occurs at *x/c*=0.665 with reattachment occurring at *x/c*=1.11. In the numerical simulations, the DES solution differs most from the experimental data. The DES separation point is at *x/c*=0.641, and its reattachment location is at *x/c*=1.35. The RANS solution is closer to the experimental observations, separating at *x/c*=0.663 and reattaching at *x/c*=1.22. The ZDES and DDES solutions are only slightly better. Separation occurs at *x/c*=.662 with reattachment at *x/c*=1.18 for both.

The boundary layer at the top of the hump in the DES solution, *x/c*=0.6, is thicker than the boundary layers that develop in the ZDES, DDES, and RANS solutions (Fig. 3, right panel), explaining the early separation. This modeling artifact is an example of Menter's (2003) grid-induced separation that results from Spalart et al.'s (2006) modeled-stress depletion. Paterson and Peltier (2005) noted this effect for DES of the trailing-edge flow of a 2D airfoil, a similar geometry to the aft side of the Glauert-Goldschmied hump.

	RANS	DES	ZDES	DDES	Exp.
Separation	0.663	0.641	0.662	0.662	0.665
Reattachment	1.22	1.36	1.18	1.18	1.11

Table 1 Separation and reattachment points for RANS, DES, ZDES, DDES and the experiment in terms of *x/c* measured from the leading edge of the hump.

The discriminator functions separating the RANS and LES regions of the DES variants are plotted in Fig. 6 for DES (left panel), ZDES (center panel), and DDES (right panel) and the wall coordinate, y^+, where the approximate transition from RANS to LES occurs is reported for an example point near the lower boundary in the separated zone at *x/c*~0.9. One sees that the LES mode is active everywhere in the DES model (Fig. 6, left panel) except very near the upper and lower boundaries, so without resolved turbulence scales, proper turbulence mixing cannot occur. In contrast, the ZDES model remains predominantly RANS (Fig. 6, center panel), except within the separated zone, providing an effective shielding of the attached boundary layers from premature transition to LES. Similar to DES, the DDES model (Fig. 6, right panel) allows a much broader LES regime than ZDES, thus the model may be more sensitive to modeled-stress depletion; however, like ZDES, a thicker RANS layer is maintained near walls, providing boundary layer shielding.

Contours of the dimensionless eddy diffusivity are plotted in Fig. 7. Prior to separation, the ZDES, DDES, and RANS solutions are similar, showing significant modeled turbulence mixing above the top of the hump, *x/c<0.6*. This contour is absent from the DES solution, confirming modeled-stress depletion in this region and supporting the premise that modeled-stress depletion is the primary cause of premature separation. Within the separated zone, the eddy diffusivities of DES, ZDES, and DDES solutions are similarly small, relative to the RANS solution, as they need to be to support resolved turbulence motions.

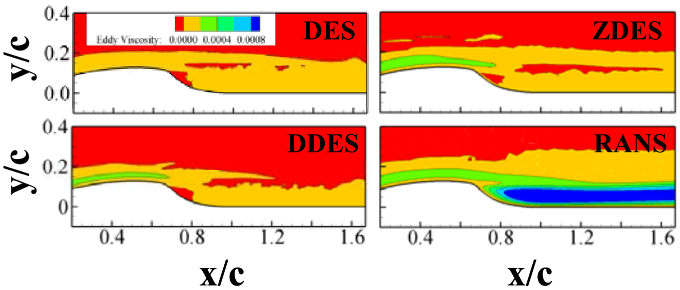

Figure 7 Eddy viscosity contours for DES, ZDES, DDES and RANS methods.

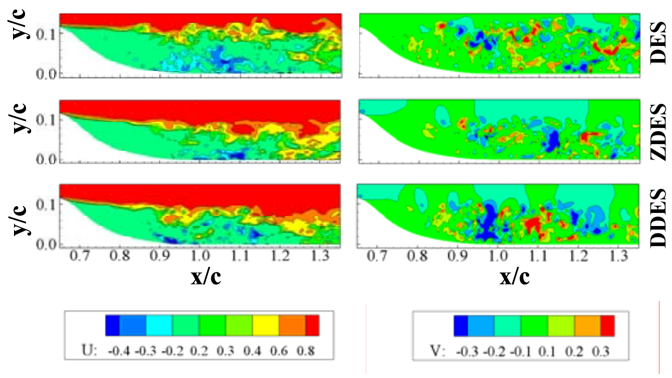

Figure 8 Contours of U and V velocities for DES, ZDES and DDES methods.

Turbulence in the resolved separated flow is visualized in Fig. 8 using contours of the streamwise (left) and vertical (right) velocities. The imprint of premature separation is observed in the shallower separation angle of the separated shear layer for the DES solution than the separation angles from the ZDES and DDES models, which are similar. The effect is the longer separation bubble predicted by DES. The DES variants show similar turbulence structures and fluctuation magnitudes in their LES zones.

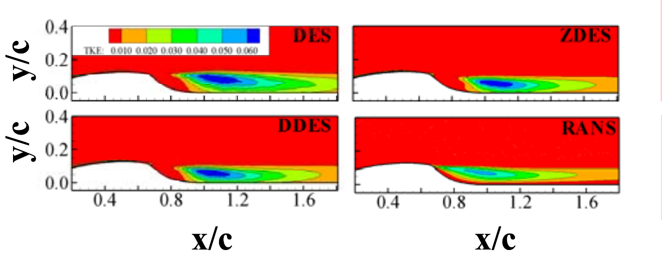

Figure 9 Contours of total turbulent kinetic energy (subfilter + resolved) for DES, ZDES, DDES and RANS.

Contours of the total turbulent kinetic energy (TKE) are presented in Fig. 9. Both resolved turbulence, superscript "*r*", and modeled subfilter turbulence, superscript "*s*", contribute to the TKE, *k*:

$$k = \frac{1}{2}\overline{u_i u_i} = \frac{1}{2}\left(\overline{u_i^r u_i^r} + \overline{u_i^s u_i^s}\right) \tag{14}$$

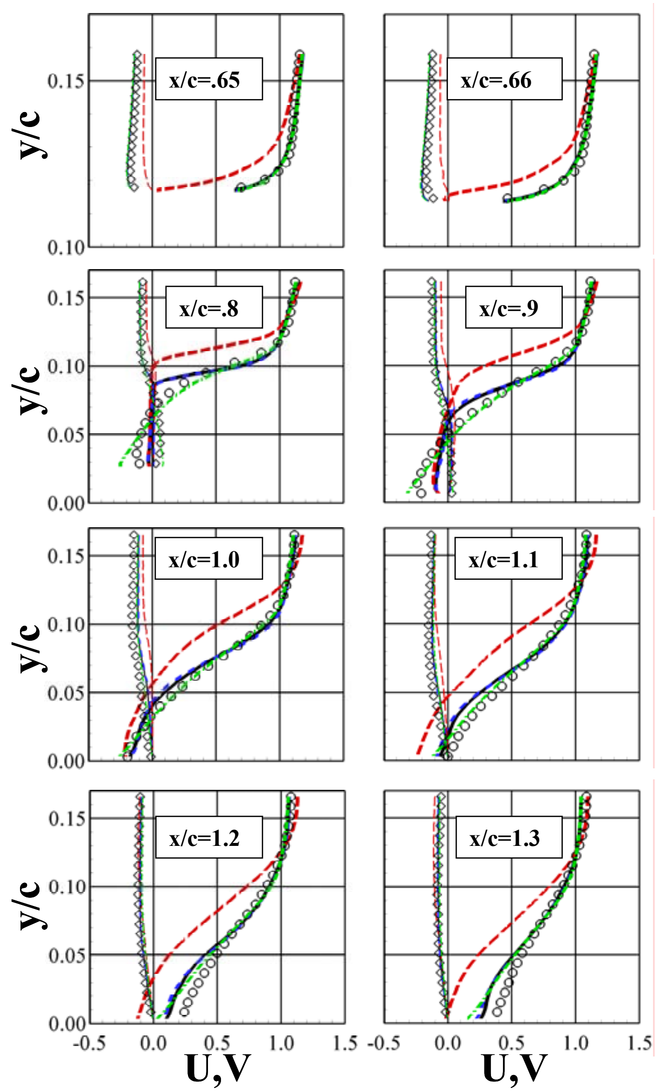

Figure 10 Profiles of U (thick) and V (thin) for DES (long dash), ZDES (dash), DDES (solid), and RANS (dash dot) at x/c locations of interest. Symbols are the experimental results for U (circle) and V (diamond).

To compute (14), the resolved TKE information is extracted from the temporally/spatially averaged flow statistics; and the subfilter information is diagnosed from the turbulence model, see (9c). TKE contours from the RANS model show significant turbulence energy within the separation and extending to the separation point. The DES-based models also predict significant TKE levels in the separated zone for x/c>0.9; however, they do not capture the TKE levels from x/c=0.6 to 0.9. Because the discriminator functions of Fig. 6 show that the region from x/c=0.6 to 0.9 lies within the LES zone and because the RANS model shows that significant turbulence motions are expected, we conclude that the loss of turbulence in the DES-based models is artifact of modeled-stress depletion; however, one for which a modeling correction has yet to be identified.

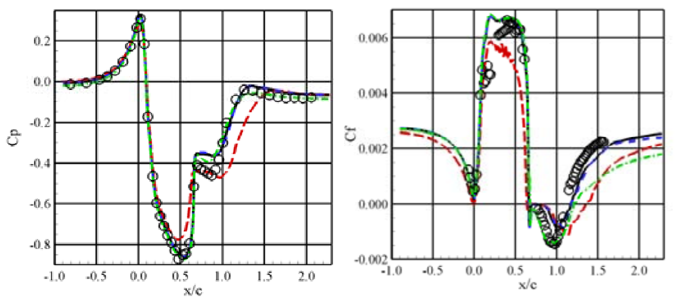

Figure 11 Pressure and skin friction coefficient profiles for DES (long dash), ZDES (dash), DDES (solid), RANS (dash dot) and experiment (circle).

Comparisons to Experimental Data

Profiles of the *U* and *V* velocities are presented in Fig. 10 for 8 stations along the flow separation (*x/c*=0.65, 0.66, 0.8, 0.9, 1.0, 1.1, 1.2 and 1.3; see Fig. 13 for details). The computational data were extracted by interpolating onto the experimental probe measurement locations. Because the DES recirculation is larger than the experimentally observed one, the relative locations within the recirculating zone of the DES extraction points (as a fraction of the recirculation length) are different from the relative locations of those extraction points in the experiment. Thus, the poor observed agreement between the DES solution and the experimental data is understood. It should be noted that Krishnan et al. (2004) present very good comparisons to the Glauert-Goldschmied data for DES; however, they had nearly twice as many grid points and enforced RANS to a point slightly upstream of the flow separation to avoid adverse effects of transition from RANS to DES in the upstream boundary layer, thus providing a boundary-layer shield.

Profiles from RANS and from the boundary-layer shielded ZDES and DDES models compare very well to the experimental results upstream and at the separation point (*x/c* =0.65 and 0.66). They also agree well near the eye of the separation bubble (at *x/c*=1.0 and 1.1). A mild discrepancy is observed near the surface close to the reattachment point (see *x/c*=1.2 and 1.3), only because the computational reattachment locations differ slightly from the experimental one. Serious differences from experiment are observed in the ZDES and DDES solutions in the region strongly affected by modeled-stress depletion, x/c=0.8 and 0.9. Our DES solution behaves similarly. The *U* and *V* velocities are near zero at these locations, unlike the RANS prediction and the experimental measurements.

Skin friction coefficient, C_f, and pressure coefficient, C_p, profiles along the bottom surface of the hump are presented in Fig. 11 where C_f and C_p are defined as:

$$C_f \equiv \frac{\tau_w}{\frac{1}{2}\rho U_r^2} \text{ and } C_p \equiv \frac{\left(\tilde{p} - p_\infty\right)}{\frac{1}{2}\rho U_r^2} \qquad (15)$$

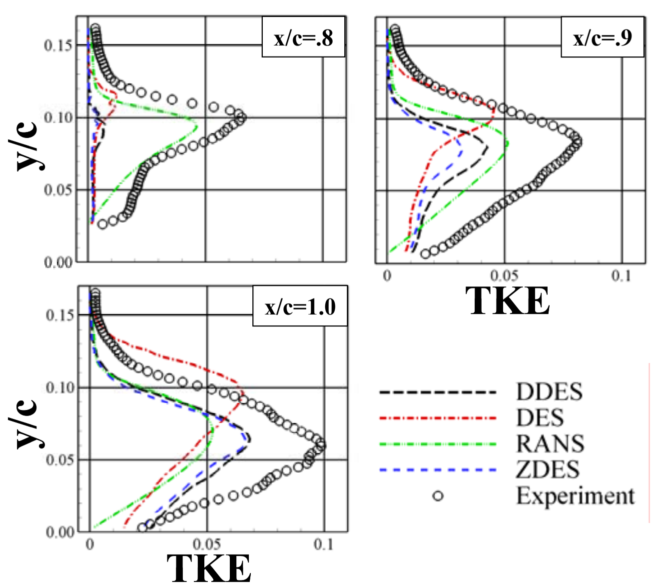

Figure 12 Plots of total turbulent kinetic energy for DES, ZDES, DDES, RANS and experiment at x/c=0.8, 0.9 and 1.0.

Because the reference pressure, p_∞, cannot be diagnosed from the incompressible flow solution, the C_p profile is adjusted by a constant computed to match the first experimental data point near *x/c*=-1. Both profiles agree well with experimental data upstream of the separation, for *x/c*<0.5, for the ZDES, DDES, and RANS solutions. A discrepancy is observed for the DES results which overpredict C_p and underpredict C_f in the range from *x/c*~0.3 to *x/c*~0.7. C_p data for the ZDES, DDES, and RANS solutions also agree well with the experiment in the pressure recovery region. Pressure recovery in the DES solution is delayed slightly, because the DES recirculation zone is longer than the experimental one. The trend in the pressure recovery, however, is correct. The modeled ZDES, DDES, and RANS data are least accurate in the region from *x/c*=0.6 to 0.9, where modeled-stress depletion is significant. The amplitudes of the DES data, however, compare well in this region; a finding, that may be fortuitous, because the upstream DES solution differs from the experimental data.

Our C_p results fall within the spread reported by Rumsey et al. (2004) summarizing contributions to the CFD Validation Workshop on Synthetic Jets and Turbulent Separation Control (see their Fig. 22a). Our DES compare well with those presented by Krishnan et al. (2004) with the exception of the delayed pressure recovery. We note that our DES solution was allowed to find its own separation point, while Krishnan et al.

(2004) enforced RANS until near the experimental separation point, an observation possibly accounting for the recirculation zone size differences.

ZDES and DDES are clearly more accurate for predicting skin friction (Fig. 11, right panel). RANS performs well until the pressure recovery region where it departs from the experimental profile. Upstream of the separation point, near x/c=0.2, the RANS, ZDES, DDES models overpredict skin friction. Biswas (2006) was able to accurately predict the skin friction in this location using LES, so the observed over-prediction may be attributed to RANS model error.

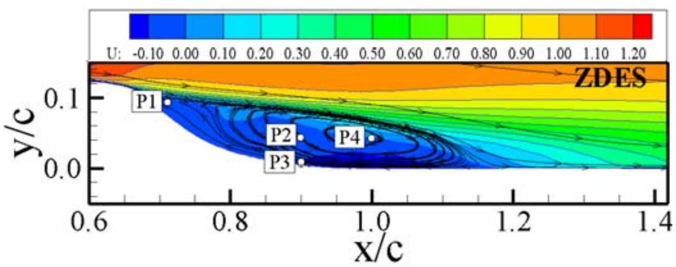

Figure 13 Points where time histories and spectra were collected at points 1, 2, 3, and 4 are shown for the ZDES case.

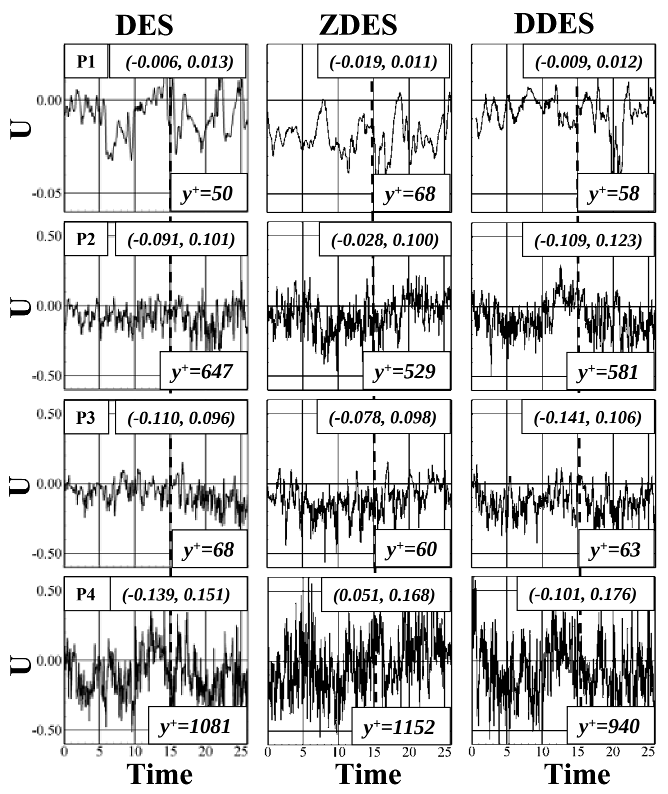

Figure 14 Time histories of U with (U_{avg}, U_{rms}) and y^+ insets. Time averaging was initiated at the dotted line.

Plots of the turbulent kinetic energy extracted from the data of Fig. 9 are presented in Figure 12. The experimental data is significantly larger than the computational results in all cases with the RANS result matching most closely. Documentation from the experiment states that there is an estimated maximum error on the experimental turbulent rms values used to calculate the experimental TKE of 14% (http://cfdval2004.larc.nasa.gov/case3expdata.html) based on a pseudo-empirical uncertainty analysis conducted by NASA. At $x/c=0.8$, the error in the RANS prediction based on peak amplitude difference is approximately 30%. The imprint of modeled-stress depletion on the DES variants is also clear. Each shows TKE values near zero. DES has slightly higher TKE levels, possibly due to the earlier separation (x/c=0.64) which allows a longer fetch for turbulence scales to develop. The upward shift in the DES profile is possibly due to the different structure of the recirculation zone. At stations x/c=0.9 and 1.0, the DES methods show TKE levels of the same order as RANS. Still the under-prediction of TKE of approximately 30% persists.

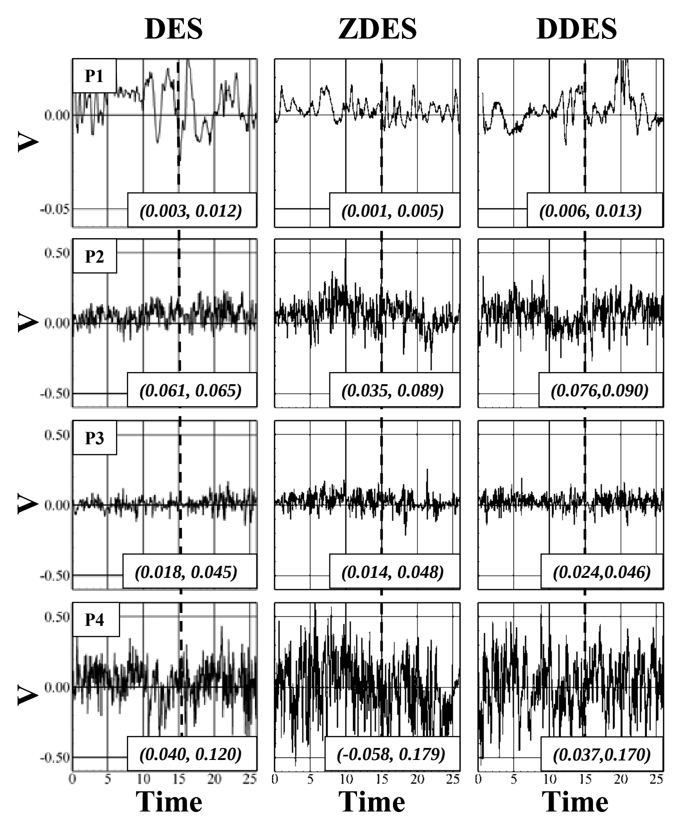

Figure 15 Time histories of V with (V_{avg}, V_{rms}) inset. Time averaging was initiated at the dotted line.

Turbulence Point Statistics

To compare the performance of the DES variants in the separated flow, time histories of 4 points were collected. Figure 13 shows their absolute locations. The vertical locations of Points 1, 2, and 4 are chosen to place them midway between the lower boundary and the upper shear layer of the separation. Point 3 is placed near the lower boundary. The horizontal location of Point 1 places it in the modeled-stress depleted region shortly downstream of separation, x/c=0.7. Points 2 and 3 are at x/c=0.9, well within the flow separation but upstream of the eye. Point 2 is near the center of the recirculating flow.

Line plots for the horizontal velocity, U, and vertical velocity, V, are shown in Figs. 14 and 15, respectively. Average and root-mean-square (*rms*) values are included in parentheses. Point 1 is the least energetic, more than a factor of 10 less active than the other locations. Point 2 shows similar activity in U and V, indicating approximate homogeneity. The *rms* values of U for Points 2 and 3 are similar, suggesting approximate homogeneity, even though Point 3 is close to the lower boundary. Sweeping velocities carry with them turbulence scale information from the larger scales above. The *rms* value of V for Point 2, however, is significantly larger than the *rms* value of V for Point 3, showing the kinematic constraint of the wall on the normal velocity. Point 4 shows considerably greater turbulence activity than the other measurement locations with the *rms* values of U and V of the same order. Flow near the core of the vortex is highly unsteady.

Power spectra for U, Φ_u, and V, Φ_v, were computed for Points 1 through 4. There is insufficient sample in the time histories to remove noise from the power spectra, so band-average smoothing was applied to each:

$$\Phi_S(\omega) = \frac{\alpha}{2\Delta\omega}\int_{\omega-\Delta\omega}^{\omega+\Delta\omega}\Phi(\omega)\,d\omega \quad (16)$$

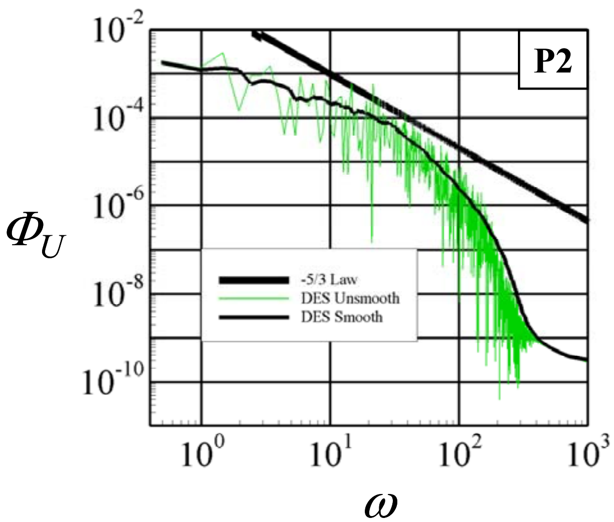

Figure 16 Raw and smoothed power spectra for U for Point 2 of the DES solution.

The band half-width, $\Delta\omega$, and rescaling amplitude, α, are chosen so that the smoothed spectrum will have the same inertial-range amplitude as the raw one. Figure 16 shows the raw power spectrum and its smoothed counterpart for the ZDES sample from Point 2. The complete set of smoothed power spectra are displayed in Fig. 17 with an $\omega^{-5/3}$ sloped line to assess the existence of inertial-range behavior. Φ_u and Φ_v are plotted together.

The spectral amplitudes of Point 1 are much smaller than the amplitudes of the other Points, in agreement with the observation that the modeled-stress depletion zone is relatively quiescent. The power spectra for Point 2 are nearly identical for DES, ZDES, and DDES suggesting that the modeling approaches perform equally well, once the separation is established. The amplitude of Φ_v for ZDES is consistently less than the amplitudes for the other models. This observation is consistent with ZDES remaining RANS longer than either DES or DDES (refer to Figs. 6 and 7), suppressing turbulence scales. The power spectra Φ_u and Φ_v depart from one another for Point 3 at low frequencies. Large scale motions are suppressed for the flux carrying eddies in the wall normal direction. Again, the DES variants perform equally well. Finally, the power spectra for Point 4 are all nearly identical showing, both, approximate homogeneity and the observation that the DES variants are performing equally well. The spectral amplitudes of the DES spectra somewhat smaller at mid frequencies, a behavior probably associated with the relative location of the longer separation zone.

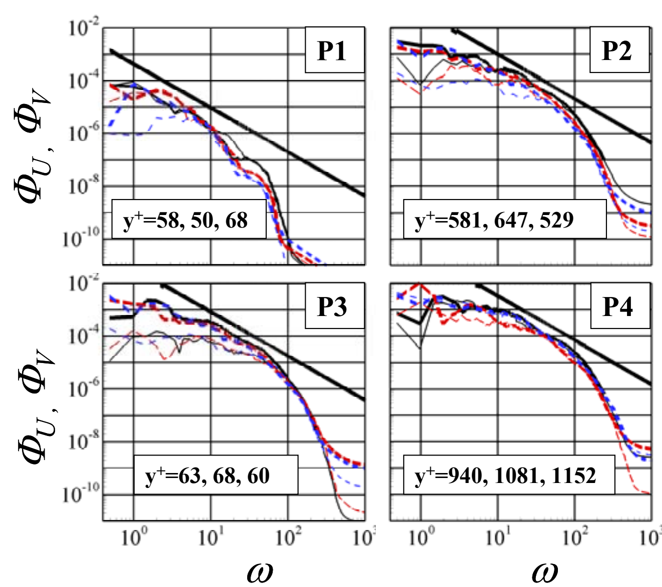

Figure 17 U and V Power Spectra for DES (long dash), ZDES (dash), and DDES (solid) with the (DDES, DES, ZDES) y^+ locations inset. Φ_U is thick, Φ_V is thin.

CONCLUDING REMARKS

Four turbulence models, RANS, DES, ZDES, and DDES, were assessed for separated flow from a flow-control hump in a turbulent boundary layer. The ZDES and DDES models which provide boundary layer shielding were shown to minimize the effects of modeled-stress depletion and grid-induced separation. Their separation point was controlled by the underlying RANS model, which performed reasonably well.

Modeled-stress depletion, however, was not fully resolved as an issue for flow modeling. The major discrepancies between experimental and numerical results were shown to be effects of modeled-stress depletion after separation and not turbulence model performance differences within the separated zone. Power spectra showed that the DES variants perform nearly equally well within the separation.

The results of this study confirm that boundary-layer shielding approaches are important for accurate prediction of separated flows using DES-based methods. The results also show that modeled-stress depletion away from attached boundary-layers remains a modeling issue for which a correction has yet to be identified.

A consideration for future research is how to avoid modeled-stress depletion in detached shear layers. One can either develop a metric to shield the flow away from boundaries from premature transition to LES or enhance the model to allow resolved turbulence scales to form earlier.

Acknowledgements

The first author is grateful for the graduate support he received through the Exploratory and Foundational Program (E&F) of the Applied Research Lab at Penn State. The authors thank Acusim Software, Inc. for supporting this work through licensing and technical assistance and acknowledge the Aeronautical Systems Center and Army Research Lab Major Shared Resource Centers where some of the computations were performed. We are grateful to Dr. Mario Trujillo and Dr. Michael Krane for helpful discussions.

References

Acusim Software Inc., 2006. “AcuSolve: A General Purpose Flow Solver”. http://www.acusim.com /images/ ACUSIM_2006 .pdf

Biswas, Debisish. 2006. Studies on Separation Control CFD Validation Test Case Based on a Higher Order LES Model. 3rd AIAA Flow Control Conference. San Francisco, Ca.

CFD Validation of Synthetic Jets and Turbulent Separation Control. Langley Research Center Workshop. 2004. http://cfdval2004.larc.nasa.gov/case3.html.

Greenblatt, D., Paschal, K. B., Yao, C., Harris, J., Schaeffler, N.W., and Washburn, A.E., 2004. “A Separation Control CFD Validation Test Case Part 1: Baseline & Steady Suction”. 2nd AIAA Flow Control Conference, Portland Oregon.

Krishnan, V., Squires, K. D., and Forsythe, J. R., 2004. “Prediction of Separated Flow Characteristic over a Hump using RANS and DES”. 2nd AIAA Flow Control Conference, Portland Oregon.

Lesieur, M., Metais, O., and Comte, P., 2005. “Large-Eddy Simulations of Turbulence,” Cambridge Univ. Press, New York.

Menter, F. R., Kuntz, M., and Bender, R., 2003, “A Scale-Adaptive Simulation Model for Turbulent Flow Predictions,” AIAA Paper 2003-0767, Reno, NV.

Naughton, J. W., Viken, S., and Greenblatt, D., 2004. “Wall Shear Stress Measurements on the NASA Hump Model for CFD Validation”. 24th AIAA Aerodynamic Measurement Technology and Ground Testing Conference, Portland Oregon.

Paterson, E.G. and Peltier, L.J., 2005, “Detached-Eddy Simulation of High-Reynolds-Number Beveled-Trailing-Edge Boundary Layers and Wakes”. Journal of Fluids Engineering, Vol. 127.

Rumsey, C.L., Gatski, T.B., Sellers, W.L., Vatsa, V.N., Viken, S.A., 2004, “Summary of the 2004 CFD Validation Workshop on Synthetic Jets and Turbulent Separation Control,” AIAA Paper 2004-2217, Portland, OR.

Seifert, L. G. Pack., 2002, “Active Flow Separation Control on Wall Mounted Hump at High Reynolds Number”. AIAA Journal, Vol. 40, No. 7.

Slimon, S., 2003, “Computation of internal separated flows using a zonal detached eddy simulation approach”. In Proceedings of the 2003 ASME International Mechanical Engineering Congress.

Spalart, P., Jou,W.-H., and Allmaras, S., 1997, “Comments on the feasibility of les for wings, and on a hybrid rans/les approach”. In Advances in DNS/LES: First AFOSR Int. Conf. on DNS/LES, C. Liu and Z. Liu, Eds., Greyden Press.

Spalart, P.R., Deck, S., Shur, M.L., Squires, K.D., Strelets, M.Kh., Travin, A., 2006. A New Version of Detached-Eddy Simulation, Resistant to Ambiguous Grid Densities. Theor. Comput. Fluid Dyn. 20:181-195.

Strelets, M., 2001, “Detached Eddy Simulation of Massively Separated Flows”. AIAA 2001-0879. 39th AIAA Aerospace Sciences Meeting and Exhibit, Reno, NV.

Tennekes, H. and Lumley, J.L., “A First Course in Turbulence,” 1972, MIT Press, Cambridge, MA. Technology and Ground Testing Conference, Portland Oregon.

